Lühr, H., Rother, M., Häusler, K., Fejer, B., Alken, P. (2012): Direct comparison of nonmigrating tidal signatures in the electrojet, vertical plasma drift and equatorial ionization anomaly. - Journal of Atmospheric and Solar-Terrestrial Physics, 75-76, 31-43

DOI: 10.1016/j.jastp.2011.07.009

Special Issue JASTP
"Atmospheric Coupling Processes in the Sun-Earth System"

(Accepted version, July 25, 2011)

Direct comparison of nonmigrating tidal signatures in the electrojet, vertical plasma drift and equatorial ionization anomaly

H. Lühr[1)], M. Rother[1)], K. Häusler[1)], B. Fejer[2)], P. Alken[3)]

1) Helmholtz Centre Potsdam, GFZ German Research Centre for Geociences, Potsdam, Germany.
2) Center for Atmospheric and Space Sciences, Utah State University, Logan, Utah, USA.
3) Cooperative Institute for Research in Environmental Science, University of Colorado, Boulder, Colorado, USA.

Abstract:

This paper presents for the first time a full decomposition of tidal signatures in three important ionospheric quantities, the equatorial electrojet (EEJ), vertical plasma drift and the crest-to-trough ratio (CTR) of the equatorial ionization anomaly. Data sources are the EEJM-2 model, ROCSAT-1 data and CHAMP electron density measurements. The analysis is based on data sampled around the solar maximum 23 (2000-2004). Full spectra of the predominant non-migrating tides were determined. The tidal component DE3 is dominating the spectrum during the months around August in all three quantities. Conversely, DE3 disappears around December solstice everywhere. The August enhancement in EEJ strength is almost 3 times larger than that in plasma drift and CTR. The DE2 tide is strong during solstice months and shows minima around equinoxes. The relative amplitudes of the annual variations are much the same for the three investigated quantities. The EEJ and the zonal wind around 100 km altitude exhibit almost identical DE2 and DE3 annual variations. Similarly, the vertical plasma drift and the zonal wind around 400 km altitude show much the same DE2 and DE3 annual variations. But their phase values are quite different, making a direct interaction less probable. Clear DE2 and DE3 tidal signature are only found in ionospheric quantities during daylight hours. There is a suite of other nonmigrating tides which can be explained by the interaction of migrating diurnal and semi-diurnal solar tides with stationary longitudinal structures. These tides are prominent during solstices and generally weak during equinoxes.

Keywords: low-latitude ionospheric dynamics, waves and tides, nonmigrating tides, thermosphere-ionosphere coupling

1. Introduction

The low **latitude** and equatorial ionosphere is characterized by a number of special phenomena and related effects. Among these is the equatorial electrojet (EEJ), an intense current in the E-layer, confined to a narrow band along the dip-equator. Prime drivers for the EEJ are the E region dynamo zonal electric field and zonal winds (Heelis, 2004). The zonal E-field at low latitudes also moves plasma upward to high altitudes. As a consequence of this fountain effect, plasma is accumulated at low latitudes forming bands of electron density maxima in the ionospheric F region north and south of the magnetic equator. This phenomenon is called the equatorial ionization anomaly (EIA).
Recently, growing evidence is provided on longitudinal modulation of ionospheric quantities by tidal effects originating from the tropical troposphere. Sagawa et al. [2005] and Immel et al. [2006] were the first who suggested a relation of the four-peaked longitudinal structure in ionospheric UV emission to the diurnal eastward propagating nonmigrating tide with zonal wavenumber 3, in short DE3. Soon thereafter England et al. [2006] reported about a wavenumber 4 longitudinal pattern of the EEJ intensity. A full analysis of the DE3 tidal signature in the EEJ was presented by Lühr et al. [2008]. In the meantime several authors have found four-peaked longitudinal structures in the vertical plasma drift [e.g. Hartmann and Heelis, 2007; Kil et al., 2007; Fejer et al., 2007]. There are even more reports on wavenumber 4 density patterns of the equatorial ionization anomaly [e.g. Lin et al., 2007; Liu and Watanabe, 2008; Scherliess et al., 2008; Wan et al., 2008]. All these studies provide a phenomenological relation of the wavenumber 4 (WN4) structure to the DE3 nonmigrating tidal component. A quantitative analysis of the role played by the various tidal components is so far missing.

Meanwhile, it is well accepted that latent heat released from deep convection in the tropical troposphere is the major source of the nonmigrating tides DE2 and DE3 [Hagan and Forbes, 2002, 2003]. These authors state that DE3 tides dominate the temperature and zonal wind response at low latitude near 100 km altitude during most of the year. In tidal terminology D stands for diurnal, S for semi-diurnal, E for eastward and W for westward propagation. The number at the end quantifies the number of wave maxima that exist simultaneously around the globe. The signatures of the DE2 and DE3 nonmigrating tide have been found to be most prominent in the MLT (mesosphere, lower thermosphere) region. Based on data from the TIMED satellite, Forbes et al. [2006, 2008] analyzed the tidal signature in temperature, and likewise Oberheide et al. [2006, 2007] retrieved the signatures in winds. Meanwhile the effects of the same tidal components have also been detected in data of the CHAMP satellite at about 400 km altitude, i.e. in zonal wind [e.g., Häusler and Lühr, 2009] and in mass density [e.g., Liu et al., 2009]. These tidal components, DE2 and DE3, in the neutral atmosphere are considered to be prime driver for related tidal signatures in ionospheric phenomena. The region of most efficient ion/neutral coupling is the E-layer. There are several modeling studies that tried to reproduce the observed tidal signatures (four-peaked longitudinal structure) in the EIA by linking it to DE3 excitation from below (e.g. Hagan et al., 2007; Jin et al., 2008; England et al., 2010). All of them confirmed the modification of the ionospheric dynamo by tidal winds, but no coherent picture of the F region electron density distribution emerged from the different simulations. This is partly due to insufficient observations that are not able to clearly reflect the complicated physics governing the plasma/neutral coupling.

Recently it was possible to express the tidal dynamics of the upper atmosphere in the form of Hough Mode Extensions (HME) [Oberheide and Forbes, 2008]. HME analysis of SABER and TIDI measurements in the MLT region showed the internal, quantitative consistency of the DE3 temperatures and horizontal winds derived from the two instruments on board TIMED. These functions are a suitable tool for predicting the signals into unsampled regions up to CHAMP altitudes. HMEs can also be used to quantify the ionospheric input. A detailed description of HMEs representing the DE3 tidal evolution of the years 2002 through 2008 is given by Oberheide et al. [2009]. Their study shows that DE3 maximizes at low latitudes, and the annual variation of the amplitude exhibits a peak around August and a minimum around December.

In this study we present a detailed tidal analysis of longitudinal structures in the equatorial electrojet, the vertical plasma drift and in the equatorial ionization anomaly. For this we make use of measurements derived by the satellites ROCSAT-1 and CHAMP. In the beginning we focus on the months around August, as an example, when the DE3 tide is known to be largest. A detailed description of the applied analysis is given for that time period. Special effort is put in the comparison of the tidal components excited in the three considered ionospheric quantities. Furthermore, we investigate the annual variation of the different tidal components. For the tides DE2 and DE3 we try to relate the deduced amplitude variations to zonal wind observations in the MLT region and at 400 km altitude.

2. Data sets used and processing approach

Prime purpose of this study is to compare tidal signatures which are present in different ionospheric and atmospheric quantities. Relevant data have been sampled by a number of different satellites. An important data source is the CHAMP satellite launched in July 2000 into a circular, near-polar (inclination 87.3°) orbit at 456 km altitude [Reigber et al., 2002]. By the end of 2009 the orbit had decayed to a height of ~300 km. The mission ended in September 2010. Due to the chosen inclination the orbital plane precessed through local time at a rate of 1 hour per 11 days, requiring 130 days for covering all local times when ascending and descending arcs are combined.

We make use of data from a number of scientific instruments onboard CHAMP. High-resolution magnetometers provide readings of the scalar and vector magnetic fields at a rate of 1 Hz. These are inverted in order to determine ionospheric currents. In particular, a systematic mapping of the equatorial electrojet was performed [Lühr et al., 2004]. Another important instrument is the Planar Langmuir Probe (PLP). It provides estimates of the electron density and electron temperature every 15 s [Cooke et al., 2003]. Readings of this instrument have been used for deriving latitudinal electron density profiles and in particular to map the equatorial ionization anomaly (EIA). From the tri-axial Accelerometer (ACC) measurements the thermospheric density and cross-track wind can be deduced [Doornbos et al., 2010]. Preprocessed data of this instrument are averages over 10 s.

The ROCSAT-1 satellite was orbiting the Earth at an altitude of 600 km and an inclination of 35°. Data considered here are from the Ionospheric Plasma and Electrodynamic Instrument (IPEI) [Ye et al., 1999]. This probe is able to measure among others the cross-track ion velocity. Averages over 15 s of the vertical plasma drift in the vicinity of the magnetic equator are considered in this study. Reliable data are available from June 1999 through June 2004.

2.1. Data sets

In this section we shortly describe the various data sets, where the subsequent tidal wave analysis is based on.

2.1.1 Equatorial electrojet

Here we make use of the empirical EEJ model developed by Alken and Maus [2007]. This model returns the peak EEJ sheet current density at the equator when provided with time, longitude and solar flux index (F10.7). Data of the first model version, EEJM-1, were utilized in an initial study investigating the influence of the nonmigrating tide DE3 on the electrojet [Lühr et al., 2008]. EEJM-1 did not allow for resolving the seasonal differences between spring and fall equinoxes. As more CHAMP data became available this limitation was removed in the second version, EEJM-2, and in addition, the influence of the moon phase is considered as well. The new EEJ model is accessible at http://www.geomag.us/models/EEJ.html. For our study we utilize current densities derived from the latest model version.

2.1.2 Vertical plasma drift

A model of the vertical plasma drift at 600 km altitude, at dip-equator latitudes, has been derived by Fejer et al. [2008] from ROCSAT-1 observations. This model is not represented in form of mathematical functions but as a series of tables. The solar flux is binned in steps of 10 sfu (solar flux unit: 10^{-22} W/m^2 Hz) over the range F10.7 = 100-200 sfu. Data are sorted into 24 overlapping longitude bins each 20° wide and the local time variations are represented by 1.5 hour bins advanced by 1-hour steps. Samples from quiet times (Kp $\leq$ 3) during the years June 1999 through June 2004 have entered the model. In order to ensure a high reliability of the model, included samples had to pass special selection criteria [see Fejer et al., 2008]. For our study of tidal signals we make use of this data set. The analysis presented here is based on a series of longitude versus local time tables one for each of the 12 months of a year. We consider plasma drift readings over the solar flux range F10.7 = 120-180 sfu. For the tidal analysis only data from daylight hours are taken into account.

2.1.3 Equatorial ionization anomaly

Another quantity we investigated here is the electron density in the low latitude F region. For our analysis we consider CHAMP readings of the PLP taken along meridional profiles between ±40° magnetic latitude. Rather than directly interpreting the electron density profiles we compute the crest-to-trough ratio (CTR) as an index for characterizing the EIA intensity. This approach was earlier applied by Lühr et al. [2007] and by Mendillo et al. [2000] for total electron content (TEC) studies.

$$CTR = \frac{1}{2}\frac{n_{cn} + n_{cs}}{n_t} \qquad (1)$$

where n_{cn} and n_{cs} are the peak electron densities at the northern and southern EIA crest and n_t is the density at the equatorial trough. For each pass of CHAMP the EIA is thus characterized by a single number. In case no anomaly has formed, CTR is set to 1. The CTR index can be regarded as a measure for the strength of the equatorial ion fountain.

For the study presented here CHAMP data from quiet times (Kp < 3.5) during the years Aug. 2000 to Aug. 2005 have been considered. Over a 5-year period CHAMP provides just an even distribution of local time sampling of all seasons. The average solar flux was F10.7 = 145 ±46 sfu. For the first studied interval, i.e. the three months around August, data came from the time 1 July to 10 Oct. 2001. During that period the solar flux level was quite high varying around F10.7 = 178 ±35 sfu.

Over the 5 years considered the CHAMP altitude decayed from 450 to 370 km. At the same time the F region height became lower, due to the declining solar cycle. Stolle et al. [2008] have shown in their Figure 1 that the shape of the EIA as sampled by CHAMP has not changed significantly over the covered height range. We therefore assume that the orbital decay of CHAMP is not influencing the tidal results obtained for CTR.

2.1.4 Zonal wind

Thermospheric zonal winds at altitudes around 400 km have been measured by CHAMP. In a comprehensive study, Häusler and Lühr [2009] investigated the nonmigrating tidal signals in the upper thermospheric zonal wind at equatorial latitudes. For their analysis they considered CHAMP data from the years 2002 through 2005. This long and continuous data set enabled them to retrieve the full tidal spectrum for the diurnal and semi-diurnal components. In our study we will refer to the results presented by Häusler and Lühr [2009].

For completeness, also the tidal signals in the zonal wind at MLT altitudes are considered. Here we take advantage of the analyzed data from the TIDI instrument on TIMED [Oberheide et al., 2006; Pedatella et al., 2008].

2.2 Analysing tidal signals

Harmonic longitudinal structures observed by near-polar orbiting satellites can be caused by a multitude of tidal components. A general mathematical formulation of the relation between longitudinal patterns in satellite observations and the nonmigrating tidal description in the Earth-fixed frame is given by Forbes et al. [2006] or by Häusler and Lühr [2009] in their sections 2. For example, a wavenumber 4 structure can be caused by the diurnal tides DE3 and DW5 or the semi-diurnal tides SE2 and SW6 as well as by the stationary planetary wave sPW4.

For the actual determination of the tidal signals we first subtract the longitudinal mean value separately for all local times from the measurements. These mean-free data are further processed by spectral analysis. In case of thermospheric quantities like temperature, density and wind, homogenous data sets are available for all 24 local time hours. In those cases a 2-D Fourier transform can be applied [e.g., Häusler and Lühr, 2009] in order to uniquely determine the various tidal components. Things are more complicated in case of tidal signatures in ionospheric quantities because the electrical conductivity varies a lot over a day. Therefore we limit our investigations to daylight hours. The variation of the conductivity is accounted for by normalizing the amplitudes with a local time dependent function. This truncated and normalized data set does not allow for a straight forward application of the 2-D Fourier transform. In stead we Fourier transform the longitudinal variations for every local time and then synthesis from the Fourier coefficients the signal distribution of wavenumbers 1 to 4. Tidal amplitudes are estimated by fitting the related wave functions to the data distribution individually for each wavenumber. This process is to a certain degree subjective and non-unique since the results depend on the choice of tidal components included in the fit. Being aware of this complication we deliberately limit the number of fitted tidal components to two per wavenumber. We first estimate from the tilt angle of the phase front in the longitude vs. LT plot (cf. Fig. 3) the strongest tidal component. After fitting and subtracting this tide we inspect the residuals and chose the tidal component that fits them best. Subsequently, both these components are fitted simultaneously.

3. Tidal signatures in ionospheric quantities

In this study we will investigate the prime tidal signals in the EEJ, the vertical plasma drift and in the equatorial ionization anomaly. In particular, we want to compare the prominent features among the quantities. These may contain hints about coupling mechanisms. Some salient features of the EEJ tidal modulation have earlier been presented by Lühr et al. [2008]. As an example of our tidal analysis, we present in this section results of the time period when the DE3 tide is known to exhibit its largest amplitudes during the 3 months around August [see e.g. Pendatella et al., 2008; Häusler and Lühr 2009].

As stated above, the first step in data processing is the removal of the longitudinal mean value. Figure 1 shows the diurnal variation of this value for the vertical drift above the equator and for the CTR of the ionization anomaly. Corresponding curves for the EEJ have been presented by Lühr et al. [2008] (see their Fig. 3). The mean plasma drift at 600 km altitude peaks at a value of 19 m/s around 11 LT. After a gradual decay it reaches a minimum at 16 LT, before it starts to rise towards the pre-reversal enhancement. The crest-to-trough ratio shows a similar evolution with a peak value of 1.66 around 13 LT. The CTR mirrors in general plasma drift variations, but every thing appears about two hours later in local time. Such a delayed response of the CTR has earlier been reported by Stolle et al. [2008].

When the longitudinal mean has been removed from the data the tidal signal shows up more clearly. In Figure 2 the longitudinal structures of the residuals are shown versus local time for the EEJ, plasma drift and CTR of the ionization anomaly. The EEJ in the top panel exhibits a very prominent WN4 (wavenumber 4) longitudinal structure in August. The slight eastward tilt of the wave feature is a clear sign for the relation to the DE3 tidal component, as has earlier been shown by Lühr et al. [2008]. The interpretation of the signal distribution in the two lower frames in terms of tidal waves is less obvious. A WN4 structure, however, can be identified in both frames, but there seems to be a significant amount of interference taking place between different tidal components. Overall, the two lower frames show similar features. The wave maxima appear at similar longitudes. As expected, regions of more intense ionization anomaly (larger CTR) coincide with enhanced upward plasma drift. Rather outstanding values for CTR are observed in the Indonesian sector (Fig. 2, bottom frame). Here the EIA is particularly well developed during the hours past noon. This implies a constructive interference of several tidal components at that time and location.

In order to obtain a more quantitative picture of the tidal signatures in ionospheric quantities we investigated the spectral content of the signals shown in Figure 2. For determining the amplitudes and phases of the most prominent tidal components we fitted harmonic functions to the data within the local time interval 08 LT through 16 LT. Outside that time sector the coupling between ions and neutrals in the E region is regarded to be weak.

3.1 Spectral analysis of ionospheric tides

As a first step of the analysis we decomposed the longitudinal variations for each local time bin into the first four wavenumbers. Figure 3 shows the distribution of wave amplitude in a longitude versus local time frame separately for the electrojet, the vertical plasma drift and the crest-to-trough ratio of the EIA. This gives already a good indication of the tidal wave content in the considered quantities. The WN3 and WN4 patterns of all three quantities, as presented in Figure 3b, are dominated by eastward tilted features. The tilt angles indicate the importance of DE2 and DE3 tidal signals. There is a local time dependence of the wave amplitude in all four harmonics shown in Figure 3. In particular for the EEJ and the CTR largest amplitudes are reached around noon, which reflect the E-layer conductivity and F region electron density changes over a day, respectively. In order to compensate for these diurnal variations, we normalize the amplitudes by means of a suitable function as used in Lühr et al. [2008]. The motivation for using $[\cos\{\pi/12(LT - t_0)\}]^{1/2}$, where t_0 is the local time of the peak amplitude, is that it reflects the solar zenith angle dependence of the electron density when assuming a Chapman layer. Suitable values for t_0 are 12:30 LT and 13:30 LT for the EEJ and CTR, respectively.

For obtaining quantitative results we fitted harmonic functions to the normalized data in each panel of Figure 3. As shown by Häusler and Lühr [2009] in their Table 1, many different tidal components can contribute to each of the four longitudinal harmonics considered. In order to reduce the ambiguity of the results we fitted only up to two most prominent tidal components to each frame in Figure 3. In particular, this is DE3 for WN4, DE2 for WN3, DW3 for WN2, D0 and SW3 for WN1. The choice of analyzed tides has been described in section 2.2 and is the same for all ionospheric quantities. As a quality measure for the obtained tidal results we compare the derived wave amplitude with the root mean square (RMS) of the remaining residuals after fitting. All the results are listed in Table 1.

Table 1: Derived amplitudes and phases for the major nonmigrating tidal components in ionospheric parameters during the months July, August, and September.

Tidal	EEJ			Plasma drift			CTR		
component	Ampl. [mA/m]	(RMS)	Phase [h]	Ampl. [m/s]	(RMS)	Phase [h]	Ampl. [ratio]	(RMS)	Phase [h]
DE3	32.5	(7.5)	10.8	4.02	(0.9)	10.5	0.196	(0.052)	11.9
DE2	10.1	(3.3)	12.5	3.21	(1.2)	14.2	0.143	(0.072)	16.1
DW3	14.4	(5.7)	23.3	1.48	(1.9)	00.8	0.131	(0.08)	01.7
D0	16.6	(8.7)	23.5	3.76	(3.1)	12.6	0.147	(0.069)	05.2
SW3	7.7		14.8	5.42		13.3	0.172		16.4

The phases denote the time at which the crest of the tidal wave crosses the Greenwich meridian. In our analysis we have also taken into account the amplitude reduction due to data binning. Following the error estimates of Häusler and Lühr [2009] the amplitudes of the diurnal tides D0, DW3, DE2, DE3 had to be enhanced in our case by 1%, 3%, 5%, 9%, respectively, for the vertical drift and the CTR. In case of the semi-diurnal tide the underestimation of SW3 was 3% (S0: 5%). For the EEJ results no damping is assumed since data are derived from a model and we did not perform any binning.

From the numbers listed in Table 1 we see that the tidal components selected, in general, explain the longitudinal structures of the ionospheric quantities rather well. In most cases the signal amplitudes are more than 3 times larger than the RMS of the residuals. An exception makes DW3, where the RMS is relative large or even surmounting the wave amplitude. This tidal component is obviously not so well supported by the data. On the other hand, the resulting phases are rather similar for all three quantities, which again provide support for the validity. DE3 largely dominates the spectrum of the EEJ tidal signals during the considered season. Also in the other two quantities DE3 is the dominating tide. An exception makes SW3 which is quite prominent in the plasma drift. A discussion of that tidal component will be given in section 5.2.

4. Annual variation of tidal components

After having taken a close look at the tidal influence on the three ionospheric quantities during late summer when the DE3 forcing is known to peak, we turn now to the annual variation of the various tidal components in the electrojet, vertical plasma drift, and crest-to-trough ratio of the EIA. For the three quantities, 12 data sets are compiled centered at the middle of each month. As before, we make use of the EEJM-2 model at the desired epochs for generating the electrojet data. The solar flux is set t F10.7 = 150 sfu. In case of vertical plasma drift, the ROCSAT-1 measurements from 5 years are sorted into monthly bins. Here we consider all readings within the solar flux range F10.7 = 120-180 sfu. CTR values, derived from CHAMP data of the first 5 years, are also sorted into monthly bins. Their mean solar flux level is F10.7 = 145 sfu with a standard deviation of ±46 sfu. The tidal analysis follows the same approach as described in section 2.2. We obtain significant amplitudes (above RMS level) for the nonmigrating tides DE3, DE2, DW4, DW3, D0, S0, SW3 over major parts of a year.

The derived annual variations of the DE2 and DE3 amplitudes in the EEJ, plasma drift and CTR data are shown in Figure 4. The curves clearly confirm the dominance of DE3 during the months around August. This peak is much more prominent in the EEJ than in the plasma drift. For CTR the enhancement is in between that of the two quantities. The well-known minimum of DE3 around December solstice is present in all three cases. By comparing Figure 4 with the annual variation of DE3 in the EEJ reported by Lühr et al. [2008] (their Fig. 6) one clearly sees the improvement of the EEJM-2 model over the previous version. March and September equinoxes are no longer forced to be equal. This reveals the big asymmetry of DE3 between the two equinoxes. DE2 amplitudes are on average smaller than those of DE3, and they exhibit a different annual variation. For DE2 we find largest amplitudes around solstices and minima at equinox seasons. A similar characteristic has been shown by Pedatella et al. [2008] for the MLT zonal wind. In case of CTR the peaks in DE2 appear to be shifted to later times by about two months. The difference in annual variation between DE2 and DE3 can be explained by the longitudinal distribution of land and sea together with the preferred occurrence of thunderstorms during the different seasons.

The phases of the two tidal signals, as shown on the right side of Figure 4, do not vary much (±2 h) over the course of a year. They stay close to the times listed in Table 1. There is an indication of a small annual variation. DE2 and DE3 are varying in anti-phase. This feature is reflected well by the EEJ and the CTR. The annual averages are about the same for EEJ and plasma drift. For CTR the times are 1 to 2 hours later.

Another characteristic number is the ratio between the tidal amplitude and the longitudinally averaged background signal. For the calculation of the ratio we take the peak value of the diurnal signal (see Fig.1) from every month. In case of CTR we use $CTR_{aver} - 1$ for the background since $CTR = 1$ means no EIA observed. As can be seen in Figure 5, during the months of June to October the DE3 amplitude contributes a good fraction to the total signal. For the EEJ the wave amplitude reaches 50% of the background current density in August. For the plasma drift it is only slightly more than 20%. With 25% for CTR the DE3 amplitude is again between the two others. This comparison shows how much more prominent the DE3 is in the EEJ. The situation is different for the DE2 tide. Here the relative tidal amplitudes are quite comparable for all three quantities. Only around vernal equinox the curves deviate somewhat.

The annual variations of other prominent tidal components have also been analyzed. Further wave components determined are the diurnal DW4, DW3 and D0. Prominent semi-diurnal tides are SW3 and S0. All these nonmigrating tidal components can be generated by an interaction of the migrating solar diurnal and semi-diurnal tides with various stationary planetary waves or longitudinal structures. Figure 6 combines the annual variations of all components in tidal spectra separately for the EEJ, vertical plasma drift and CTR. This figure clearly shows the difference in characteristics between the DE2 and DE3 tides on the one hand and all the remaining tidal components on the other. The derived westward propagating and standing tides generally maximize around solstices.

We have chosen the colour code of Figure 6 in a way that reliable amplitude values start from dark blue. The standard deviations of the residuals after the fitting process have values blow

10 mA/m, 2 m/s and 0.08 for the EEJ current density, plasma drift velocity and CTR, respectively.

5. Discussion

In this paper we have investigated nonmigrating tidal signatures in ionospheric quantities. The purpose of the study is twofold, (1) compare the tidal signatures derived from the three quantities with each other and (2) try to describe the chain of processes from neutral atmosphere dynamics to ionospheric wave patterns. The variations of the electrojet, the vertical plasma drift and the ionization anomaly were derived from data of different spacecraft taken neither at the same location nor at the same time. We have taken a statistical approach to obtain comparable signatures. For solar tidal waves, when data are synchronized by Earth's rotation, such an approach can be regarded as justified.

5.1 Comparing the ionospheric tidal signals

Our first analysis is limited to the three months around August. This period was chosen because at that time nonmigrating tides excited by deep tropical convection are strongest at MLT altitudes. For completeness we have analyzed also other prominent tidal signatures occurring during that period. The EEJ is probably the phenomenon closest connected to the equatorial wind field in the MLT region. Therefore we will discuss it first. According to Table 1 we see that the DE3 amplitude is by far the largest compared to the other tidal components. In particular, DE3 is 3 times larger than DE2. This ratio is about the same as found for DE3/DE2 of zonal wind in the MLT [Pedatella et al., 2008]. All the other tidal components have amplitudes half as large as DE3 or less.

In case of the other two quantities, vertical plasma drift and CTR, the amplitudes of DE3 and DE2 do not differ that much. This is significantly different from the behavior of the EEJ. Possible reasons for that will be discussed in the next section. The longitudinal structures with wavenumber 2 are not too well represented by DW3, as can be judged from the comparison between amplitudes and RMS. But there is no other single tidal component that provides better results. The wavenumber 1 pattern has been decomposed into D0, a breezing of the atmosphere, and the semi-diurnal SW3. In particular for the plasma drift SW3 is very prominent.

In general, we find a close correspondence between the tidal components in plasma drift and CTR. This is further supported by a consistent phase shift between the two quantities. For the CTR the times when the wave crests cross the Greenwich meridian are systematic later by 1 to 3 hours compared to the plasma drift. This difference is in agreement with the delayed response of the ionization anomaly by about 2 hours with respect to plasma drift variations, as deduced from comparison of satellite and radar measurements at Jicamarca [Stolle et al., 2008]. The wave D0 makes an exception. Here the phases are significantly different in all three cases. Obviously, this component is not excited by a common tidal source.

After having shown the close relation between plasma drift and CTR we will now compare the EEJ with the vertical drift velocity. The phase values determined for DE3 are in good agreement between the two signals, and the EEJ phase fits also well the value reported by Lühr et al. [2008] in their Table 1. The phases of DE2 in EEJ and plasma drift are also in reasonable agreement. Both tidal components DE2 and DE3 have been shown to be excited by deep tropical convection [e.g. Hagan and Forbes, 2002]. For that reason it is surprising to find such a big difference in the amplitude ratio DE2/DE3 between the two quantities EEJ and vertical plasma drift. We will revisit this issue in the next section.

The interpretation of the wavenumbers 1 and 2 in terms of tidal signals is not so straight forward because the harmonic signatures in the three quantities have rather complex structures (see Fig. 3a). Even though DW3 explains only part of WN2, the phases are quite consistent between the ionospheric quantities, providing support for the significance of this tidal component. In the wavenumber 1 the semi-diurnal component SW3 plays an important role in all three quantities. The consistent phase values suggest a common source for excitation. The latter nonmigrating tidal component is probably caused by an interaction of the semi-diurnal migrating tidal wave with a wavenumber 1 stationary structure. According to the scheme for generating secondary waves, as outlined by Häusler and Lühr [2009] in their section 5, we may write for the various observed tidal components:

DW4 = DW1 + sPW3

DW3 = DW1 + sPW2,

D0 = DW1 – sPW1,

S0 = SW2 – sPW2,

SW3 = SW2 + sPW1

where sPW1, sPW2 and sPW3 are stationary planetary waves with zonal wavenumbers 1, 2 and 3, respectively; DW1 and SW2 are the migrating diurnal and semi-diurnal tides. In the cases considered here sPW1, for example, represents conditions that favor or suppress the generation of the ionospheric effects over longitudinal arcs of 180°. For the EEJ sPW1 and sPW2 may reflect the efficiency of converting MLT tidal winds into electric currents. It can be expected that the longitude range of the favorable conditions, e.g. high collision frequency and enhanced electron density, changes with season due to the deviation of the dip-equator from the geographic equator. For the vertical plasma drift other processes and also other latitudes, away from the dip-equator, are important for the conversion of MLT winds into F region electric fields.

The analysis of data for the months of July, August, September has revealed the close relation of the tidal signals in the three ionospheric phenomena. We may distinguish between two groups. WN1 and WN2 seem to be generated primarily by interaction of the migrating tides with longitudinal structures. Different from that the tidal components DE2 and DE3 are excited by deep tropical convection in the troposphere and exhibit a distinctly different seasonal variation. These two tidal components are at the center of our interest.

5.2 The seasonal variation of tidal components

By studying the tidal wave variations over the course of a year we may obtain information about their generation mechanism. Since it has been shown here that the vertical plasma drift and the crest-to-trough ratio of the EIA are closely related, we may expect similar annual variation for both quantities.

The DE2 and DE3 tidal components cause prominent modulations of the zonal wind which obtain largest amplitudes in the mesosphere, lower thermosphere region at low latitudes [e.g. Oberheide et al., 2009]. These winds can generate currents in the ionospheric E-layer. It is expected that the electrojet reflects best the signature of the wind field at the magnetic equator. In Figure 7 (top frame) we have plotted the annual variation of DE2 and DE3 amplitudes in zonal wind at 100 km altitude, as published by Pedatella et al. [2008]. There is a remarkable one-to-one agreement between the seasonal variations of the two tidal components in the electrojet and the MLT zonal wind. Also the ratio between the DE2 and DE3 amplitudes is very much the same. This convincing match is a strong argument for a direct modulation of the electrojet by the zonal wind.

The data presented here are taken during the active years of solar cycle 23. Oberheide et al. [2009] have shown that the amplitude of DE3 in zonal wind increases towards the solar minimum at altitudes above 200 km, but at MLT heights the wind speed shows little solar cycle dependence. Another obvious result from that study is the two-year modulation of the tidal amplitude. This was related to the phase of the quasi-biannual oscillation (QBO). It would warrant a follow-up study to see, whether the tidal amplitude of the EEJ also follows these temporal details of the MLT zonal wind. Such a study, however, has to employ actual EEJ observations and cannot be based on the EEJM-2 model because the model does not consider interannual variations.

In case of the vertical plasma drift at 600 km altitude we observe a similar annual variation. Figure 4, middle panel, shows again an enhancement of the DE3 amplitude during the months of June through October. In addition there appears a secondary maximum around March equinox. The DE2 amplitude is high during solstices and exhibits minima around equinoxes, very similar to the variations of the EEJ. Interestingly, the DE3 amplitude does not dominate so much; rather it is comparable in strength to DE2 in case of the vertical plasma drift.

The DE2/DE3 annual variations of CTR are somewhere in between those of EEJ and plasma drift. The preference of peak amplitudes during equinox months is partly caused by the prominence of the EIA around equinoxes. Therefore it is more appropriate for a comparison to look at the relative amplitudes in Figure 5. There we find a more homogeneous picture of the tidal signals in the three quantities.

The phase values vary only slightly over the year (cf. Fig. 4). Even if we accept an uncertainty of one hour, an annual variation is evident. Consistently, in all three quantities the phase of DE3 is earlier during late spring than during late fall. An opposite trend is observed for the DE2 tide. During the different seasons tropospheric latent heat release takes place in different regions.

For comparison, the zonal wind along the magnetic equator, as observed by CHAMP (~400 km altitude), shows very similar annual variations of DE2 and DE3 as the vertical plasma drift does (compare Figs. 4 and 7, bottom frames). Also the ratio between DE2 and DE3 amplitudes is much the same in both cases. The difference in characteristics between EEJ and F region phenomena is further supported by Figure 5 where we show the relative amplitudes of the tidal components DE2 and DE3 with respect to the background zonal mean value. For DE2 we find approximately the same relative amplitude for all three quantities. Conversely, DE3 is much more prominent in EEJ during the months around August. It is 2.5 times larger than plasma drift and 2 times larger than CTR. During the period November through April all relative amplitudes are comparable. Obviously, DE3 decays faster than DE2 on its way upward to the topside ionosphere (thermosphere). Forbes and Garrett [1979] state, based on theoretical considerations, that DE2 has a longer vertical wavelength than DE3 and thus penetrates more efficiently into the thermosphere than DE3.

As mentioned in the Introduction, the EEJ is driven by the zonal polarization electric field and zonal wind in the E-layer. By inverting the magnetic signature of the EEJ Maus et al. [2007] have identified the roles of the E-field and the wind in driving the currents. Their approach can be used to verify the close relation between DE2/DE3 tidal signals in MLT wind speed and EEJ current density. The modulation of F region plasma drift and EIA by tidal signals is more difficult to explain. Here also other winds apart from the zonal winds at the equator play a role. Regardless of that, the consistent annual variations of the phases of all three quantities (cf. Fig. 4) strongly suggest common sources for the DE2 and DE3 tidal signatures. On average the EEJ and plasma drift phases are practically the same while CTR phases are delayed by about 2 hours. Such a delay is consistent with previous studies [e.g. Stolle et al., 2008].

We have confined our investigations of tidal signatures in the equatorial electrojet, the vertical plasma drift and the strength of the plasma fountain effect to daylight hours. The reason for that is, DE2 and DE3 signatures disappear in the EEJ after 18 LT. Also for other ionospheric phenomena like F region dynamo current or inter-hemispheric field-aligned currents a ceasing of DE3 tidal signals at sunset is reported by Park et al. [2010, 2011], respectively. Contrary to that, DE2 and DE3 tidal waves are present in MLT winds over the whole 24 hours of a day [e.g. Oberheide et al., 2006]. **This shows that the dynamic processes at E-layer altitude are**

less important after sunset. At night-time the F region dynamo dominates over the E region.

Wavemumber 4 longitudinal patterns in the equatorial ionization anomaly are observable even after sunset [e.g. Sagawa et al., 2005; Scherliess et al., 2008; Liu and Watanabe, 2008]. Their zonal motion of the wave front does no longer follow any more the expected DE3 eastward phase propagation [Jin et al., 2008], and also the seasonal variation exhibits a different pattern after sunset [Liu and Watanabe, 2008]. There have been attempts to find explanations for the longitudinal structure of the EIA during pre-midnight by modeling studies [e.g. Hagan et al., 2007; Jin et al., 2008; England et al., 2010] which consider also the effect of F region winds and the modulation of O^+ ions. So far no common consensus on the mechanism has been achieved. **With our data product, CTR, we cannot contribute much to enlighten the tidal behavior of the EIA after sunset. Due to the frequent occurrence of plasma bubbles, also termed spread-F, the derived crest-to-trough ratio is not reliable at that local time.**

The vertical plasma drift data are available for all 24 hours of a day. In order to investigate the behavior at night, a tidal analysis over the whole day was performed. Figure 8 shows as an example the wavenumber 4 pattern in a longitude versus local time frame. We have selected again the time interval around August when the DE3 tide is most prominent. Between 08 and 18 LT the wave signal follows strictly the DE3 phase propagation as indicated by the thick dashed line. At 19 LT, the peak time of the pre-reversal enhancement (PRE), WN4 practically disappears. Later some WN4 signal reappears, but is not clear how closely it is controlled by the tropospheric source. After midnight phases are completely unrelated to the DE3 signal.

For completeness we looked also into the characteristics of longitudinal structures at other wavelengths and frequencies. All of them are suggested to be generated by the interaction of the migrating tidal waves with stationary ionospheric structures. Solar migrating tides in the upper atmosphere are primarily generated in the stratosphere by UV heating and in the thermosphere by EUV heating [Heelis, 2004]. The EEJ is modulated by winds from the upward propagating tide, while plasma drift and CTR can be influenced by both, the upward propagating and in-situ tides. The complete tidal spectra presented in Figure 6 confirm our suggestion. In particular, for the EEJ we find that longitudinal asymmetries appear predominantly during solstices and largely disappear during equinoxes. A pronounced stationary WN3 structure appears in the EEJ around December solstice that generates together with the diurnal migrating tide a strong DW4 signal. During other seasons DW4 is not present in the EEJ. Already Lühr et al. [2008] reported on a strong WN3 feature in December. Similarly, a WN2 stationary structure is suggested to interact with the diurnal and semi-diurnal tides. It generates DW3 and S0 waves around June and December solstices. Interestingly, the wave phase of DW3 shift by 12 hours between June and December. This clearly indicates the seasonal influence on the longitudinal structure (e.g. Cowling conductivity). The remaining signals D0 and SW3 are assigned to an interaction between the migrating diurnal and semi-diurnal tides with a wavenumber 1 longitudinal pattern. We have no immediate explanation why the interference products appear predominantly in the diurnal component during certain months and during others in the semi-diurnal.

In the case of vertical plasma drift the resolution of the data is not as good as it is for the EEJ. Even though, some similarities appear. The tides DW4 and DW3, related to WN3 and WN2 stationary structures, peak also around December solstice. DW3 exhibits again the shift in phase by 12 hours between June and December. Particularly outstanding is the strong signal in SW3. Peak amplitudes in vertical plasma drift are attained in April, but it is strong during all months outside the December solstice. Presently we cannot provide a conclusive explanation for the large SW3 amplitudes from spring equinox through June solstice, but we suggest that the migrating semi-diurnal tide, SW2, is strong during these months at mid-latitudes.

Quite similar longitudinal patterns are observed for the crest-to-trough ratio of the EIA. A major difference with respect to vertical plasma drift is found in the tidal components D0 and SW3. They peak at quite different months of the year. We are well aware of the fact that Figure 6 does not reflect the full tidal spectra of the ionospheric quantities. Just a small number of strong nonmigrating tides have been chosen.

Finally we want to address the issue of uncertainties of the results presented. All three considered data sets have their intrinsic error bars. For the EEJ model a standard deviation of 30 mA/m is quoted by [Alken et al., 2007] reflecting the day-to-day variability. Since more than 100,000 passes are considered in EEJM-2, the uncertainty of the climatological average is of the order of 1 mA/m. Measuring the vertical plasma drift above the dip-equator accurately is a very challenging task. The authors of the applied drift model [Fejer et al., 2008] give no numbers for the uncertainty, but from their scatter plot (Fig. 1) one can estimate a standard deviation of about 10 m/s. For the systematic velocity error we guess a value of 2 m/s. The crest-to-trough ratio of the EIA can be determined reliably with an uncertainty of a few percent. The day-to-day variability, however, is quite large resulting in a typical standard deviation of 0.4. For the individual bin averages we obtain uncertainties of 0.06. When comparing these uncertainties with the tidal amplitudes shown in Figure 4, the signal-to-noise ration is sufficiently large.

Further uncertainties are introduced by extracting the tidal components from the total signal. The prime tidal component for each wavenumber signal is determined rather reliably, but the choice of the secondary components is somewhat ambiguous. Fortunately, DE2 and DE3 are both prime tides of the WN3 and WN4 longitudinal patterns. As a measure for the reliability of the derived amplitude we regard its ratio to the RMS value of the unfitted residuals. Typical RMS values are 7 mA/m, 1.5 m/s and 0.06 for the EEJ, vertical plasma drift and CTR. Amplitudes and phases have been considered reliable when the amplitudes are by a factor of 1.5 larger than the RMS.

Conclusions

In this study we have provided for the first time a full tidal decomposition of three important ionospheric quantities. The analysis is based on data from three independent sources. Data for the electrojet are derived from the empirical model EEJM-2, vertical plasma drift readings are from ROCSAT-1 measurements, and the crest-to-trough ration (CTR) of the ionization anomaly is computed from CHAMP electron density measurements. The consistency of the results among the three quantities provides confidence in the reliability of the data. The analysis is based on data sampled around the solar maximum 23 (2000-2004). Important conclusions derived are:

1) The nonmigrating tide DE3 is dominating the tidal spectrum during the months around August in EEJ, vertical plasma drift and CTR. Equivalently, DE3 disappears, as expected, around December solstice in all cases. The August enhancement in EEJ strength is almost 3 times larger than that in plasma drift and 2 times larger than that in CTR.

2) The DE2 tide is strong during solstice months and shows minima around equinoxes. The relative amplitudes of the annual variations are much the same for the three investigated quantities, suggesting a lower decay of the amplitude with height.

3) The DE2 and DE3 annual variations and relative strength between the two components are almost the same for the EEJ and the zonal wind around 100 km altitude. This perfect match suggests a direct modulation of the EEJ strength by the tidal signal of the zonal wind in the E-layer.

4) The DE2 and DE3 annual variations and relative strength between the two tidal components are almost the same for the vertical plasma drift and the zonal wind around 400 km altitude. Wave phases, however, are markedly different (compare our Table 1 with Häusler and Lühr [2009] Table 2). There are no indications for an efficient coupling between the tidal waves in plasma drift and zonal wind in the topside ionosphere.

5) The phases of the DE2 and DE3 tides show much the same annual variation for the three considered ionospheric quantities. DE2 and DE3 phases vary in anti-phase over the year by ±2 hours. On average EEJ and vertical plasma drift phases have practically the same value, while the CTR phase lags behind by about 2 hours.

6) The interaction of the migrating diurnal and semi-diurnal solar tides with stationary longitudinal structures generates various nonmigrating tidal signals in ionospheric quantities. Longitudinal asymmetries are obviously more prominent during solstices and largely disappear during equinoxes. All these interference products are westward propagating or standing nonmigrating tides.

The data presented here provide results only at a few altitude levels. Suitable physics-based models should be used for identifying the processes that transfer the tidal signal from the neutral particle dynamics to the different ionospheric quantities.

Acknowledgements. We like to thank Claudia Stolle, Jens Oberheide and Nick Pedatella for fruitful discussions about tidal signatures in the ionosphere and in the MLT region. The CHAMP mission was sponsored by the Space Agency of the German Aerospace Center (DLR) through funds of the Federal Ministry of Economics and Technology, following a decision of the German Federal Parliament (grant code 50EE0944). One of the authors (KH) is supported by the Deutsche Forschungsgemeinschaft (DFG) Priority Program “CAWSES”, SPP 1176.

References

Alken, P., Maus, S., 2007. Spatio-temporal characterization of the equatorial electrojet from CHAMP, Ørsted, and SAC-C satellite measurements. J. Geophys. Res., 112, A09305, doi:10.1029/2007JA012524.

Cooke, D.L., W. Turnbull, C. Roth, A. Morgan, and R. Redus, Ion Drift-Meter Status and Calibration, in *First Champ Mission Results for Gravity, Magnetic, and Atmospheric Studies*, (eds.) C. Reigber, H. Lühr, P. Schwintzer, 212-219, Springer, Berlin-Heidelberg, 2003.

Doornbos, E., IJssel, J., Lühr, H., Förster, M., Koppenwallner, G.: Neutral density and crosswind determination from arbitrarily oriented multi-axes accelerometers on satellites, J. Spacraft Rockets, 47(4), 580589, doi:10.2514/1.48114, 2010.

England, S. L., Maus. S., Immel, T. L., and Mende, S. B., Longitude variation of the E-region electric fields caused by atmospheric tides, *Geophys. Res. Lett.*, *33*, L21105, doi:10.1029/2006GL027465, 2006.

England, S. L., T. J. Immel, J. D. Huba, M. E. Hagan, A. Maute, and R. DeMajistre (2010), Modeling of multiple effects of atmospheric tides on the ionosphere: An examination of possible coupling mechanisms responsible for the longitudinal structure of the equatorial ionosphere, *J. Geophys. Res.*, *115*, A05308, doi:10.1029/2009JA014894.

Fejer, B. G., Jensen, J. W., and Su, S.-Y.: Quiet-time equatorial F region vertical plasma drift model derived from ROCSAT-1 observations, *J. Geophys. Res.*, *113*, A05304, doi:10.1029/2007JA012801, 2008.

Forbes, J. M., and H. B. Garrett (1979), Theoretical studies of atmospheric tides, *Rev. Geophys. Space Phys.*, *17*, 1951–1981.

Forbes, J.M., J. Russell, S. Miyahara, X. Zhang, S. Palo, M. Mlynczak, C.J. Mertens, M.E. Hagan (2006), Troposphere-thermosphre tidal coupling as measured by the SABER instrument on TIMED during July-September 2002, *J. Geophys. Res.*, *111*, A10S06, doi:10.1029/2005JA011492.

Forbes, J. M., X. Zhang, S. Palo, J. Russell, C. J. Mertens, and M. Mlynczak (2008), Tidal variability in the ionospheric dynamo region, *J. Geophys. Res.*, *113*, A02310, doi:10.1029/2007JA012737.

Forbes, J. M., S. L. Bruinsma, X. Zhang, and J. Oberheide (2009), Surface-exosphere coupling due to thermal tides, *Geophys. Res. Lett.*, *36*, L15812, doi:10.1029/2009GL038748.

Hagan, M. E. and Forbes, J. M. (2002), Migrating and nonmigrating diurnal tides in the middle and upper atmosphere excited by tropospheric latent heat release, *J. Geophys. Res.*, 107(D24), 4754, doi:10.1029/2001JD001236.

Hagan, M. E., and J. M. Forbes (2003), Migrating and nonmigrating semidiurnal tides in the upper atmosphere excited by tropospheric latent heat release, J. Geophys. Res., 108(A2), 1062, doi:10.1029/2002JA009466.

Hagan, M. E., A. Maute, R. G. Roble, A. D. Richmond, T. J. Immel, and S. L. England (2007), Connections between deep tropical clouds and the Earth's ionosphere, *Geophys. Res. Lett.*, *34*, L20109, doi:10.1029/ 2007GL030142.

Häusler, K., and H. Lühr (2009), Nonmigrating tidal signals in the upper thermospheric zonal wind at equatorial latitudes as observed by CHAMP, Ann. Geophys., 27, 2643–2652.

Hartman, W.A. and R.A. Heelis (2007), Longitudinal variations in the equatorial vertical drift in the topside ionosphere, *J. Geophys. Res.*, *112*, A03305, doi:10.1029/2006JA011773.

Heelis, R. A. (2004), Electrodynamics in the low and middle latitude ionosphere: A tutorial, *J. Atmos. Sol. Terr. Phys.*, *66*, 825– 838, doi:10.1016/j.jastp.2004.01.034.

Immel, T. J., Sagawa, E., England, S. L., Henderson, S. B., Hagan, M. E., Mende, S. B., Frey, H. U., Swenson, C. M., and Paxton, L. J.: Control of equatorial ionospheric morphology by atmospheric tides, Geophys. Res. Lett., 33, L15108, doi:10.1029/2006GL026161, 2006.

Jin, H., Y. Miyoshi, H. Fujiwara, and H. Shinagawa (2008), Electrodynamics of the formation of ionospheric wave number 4 longitudinal structure, *J. Geophys. Res.*, *113*, A09307, doi:10.1029/2008JA013301.

Kil, H., S.-J. Oh, M.C. Kelley, L.J. Paxton, S.L. England, E. Talaat, K.-W. Min, and S.-Y. Su (2007), Longitudinal structure of the vertical **E**x**B** drift and ion density seen from ROCSAT-1, *Geophys. Res. Lett., 34,* L14110, doi:10.1029/2007GL030018.

Lin, C. h., W. Wang, M.E. Hagan, C.C. Hsiao, T.J. Immel, M.L. Hsu, J.Y. Liu, L.J. Paxton, T.W. Fang, and C.H. Liu (2007), Plausible effect of atmospheric tides on the equatorial ionosphere observed by the FORMOSAT-3/COSMIC: Three-dimentional electron density structures, *Geophys. Res. Lett., 34,* L11112, doi:10.1029/2007GL029265.

Liu, H., H. Lühr, and S. Watanabe, 2007. Climatology of the equatorial thermospheric mass density anomaly, *J. Geophys. Res.,* 112, A05305, doi:10.1029/2006JA012199.

Liu, H., M. Yamamoto, and H. Lühr (2009), Wave-4 pattern of the equatorial mass density anomaly: A thermospheric signature of tropical deep convection, Geophys. Res. Lett., 36, L18104, doi:10.1029/2009GL039865.

Lühr, H., S. Maus, and M. Rother, The noon-time equatorial electrojet, its spatial features as determined by the CHAMP satellite, *J. Geophys. Res.*, *109*, A01306, doi:10.1029/2002JA009656, 2004.

Lühr, H., Häusler, K., and Stolle, C.: Longitudinal variation of F region electron density and thermospheric zonal wind caused by atmospheric tides, Geophys. Res. Lett., 34, L16102, doi:10.1029/2007GL030639, 2007.

Lühr, H., Rother, M., Häusler, K., Alken, P., and Maus, S.: The influence of nonmigrating tides on the longitudinal variation of the equatorial electrojet, J. Geophys. Res., 113, A08313, doi:10.1029/2008JA013064, 2008.

Maus, S, P. Alken, and H. Lühr (2007), Electric fields and zonal winds in the equatorial ionosphere inferred from CHAMP satellite magnetic measurements, *Geophys. Res. Lett.*, *34,* L23102, doi:10.1029/2007GL030859.

Mendillo, M., L. Bosheng, and J. Aarons (2000), The application of GPS observations to equatorial aeronomy, *Radio Sci., 35*, 885– 904.

Oberheide, J., Q. Wu, T. L. Killeen, M. E. Hagan, and R. G. Roble (2006), Diurnal nonmigrating tides from TIMED Doppler Interferometer wind data: Monthly climatologies and seasonal variations, *J. Geophys. Res.*, *111*, A10S03, doi:10.1029/2005JA011491.

Oberheide, J., Q. Wu, T. L. Killeen, M. E. Hagan, and R. G. Roble (2007), A climatology of nonmigrating semidiurnal tides from TIMED Doppler Interferometer wind data, J. Atmos. Sol. Terr. Phys., 69(17–18), 2203– 2218, doi:10.1016/j.jastp.2007.05.010.

Oberheide, J., and J. M. Forbes (2008), Tidal propagation of deep tropical cloud signatures into the thermosphere from TIMED observations, *Geophys. Res. Lett., 35*, L04816, doi:10.1029/2007GL032397.

Oberheide, J., J. M. Forbes, K. Häusler, Q. Wu, and S. L. Bruinsma (2009), Tropospheric tides from 80 to 400 km: Propagation, interannual variability, and solar cycle effects, *J. Geophys. Res., 114,* D00I05, doi:10.1029/2009JD012388.

Park, J., H. Lühr, and K. W. Min (2010), Characteristics of F-region dynamo currents deduced from CHAMP magnetic field measurements, *J. Geophys. Res.*, 115, A10302, doi:10.1029/2010JA015604.

Park, J., H. Lühr, and K. W. Min (2011), Climatology of the inter-hemispheric field-aligned current system in the equatorial ionosphere as observed by CHAMP, Ann. Geophys., 29, under review.

Pedatella, N. M., J. M. Forbes, and J. Oberheide (2008), Intra-annual variability of the low-latitude ionosphere due to nonmigrating tides, Geophys. Res. Lett., 35, L18104, doi:10.1029/2008GL035332

Reigber, C., H. Lühr, and P. Schwintzer (2002), CHAMP mission status, *Adv. Space Res., 30,* 129–134.

Pancheva, D. and P. Mukhtarov (2010), Strong evidence for the tidal control on the longitudinal structure of the ionospheric F-region, *Geophys. Res. Lett.*, 37, L14105, doi:10.1029/2010GL044039.

Sagawa, E., Immel, T. J., Frey, H. U., and Mende S. B.: Longitudinal structure of the equatorial anomaly in the nighttime ionosphere observed by IMAGE/FUV, J. Geophys. Res., 110, A11302, doi:10.1029/2004JA010848, 2005.

Scherliess, L., D. C. Thompson, and R. W. Schunk (2008), Longitudinal variability of low-latitude total electron content: Tidal influences, J. Geophys. Res., 113, A01311, doi:10.1029/2007JA012480.

Stolle, C., C. Manoj, H. Lühr, S. Maus, and P. Alken (2008), Estimating the daytime Equatorial Ionization Anomaly strength from electric field proxies, J. Geophys. Res., 113, A09310, doi:10.1029/2007JA012781.

Yeh, H.-C., S. Y. Su, Y. C. Yeh, J. M. Wu, R. A. Heelis, and B. J. Holt (1999), Scientific mission of the IPEI payload onboard ROCSAT-1, Terr. Atmos. Ocean, 19–42, supplementary issue.

Wan, W., L. Liu, X. Pi, M.-L. Zhang, B. Ning, J. Xiong, and F. Ding (2008), Wavenumber-4 patterns of the total electron content over the low latitude ionosphere, Geophys. Res. Lett., 35, L12104, doi:10.1029/2008GL033755.

Figure captions

Figure 1: Zonally averaged diurnal variation: *(top)* vertical plasma drift, *(bottom)* crest-to-trough ratio of the equatorial ionization anomaly.

Figure 2: Local time dependence of the longitudinal variation during the months around August: *(top)* equatorial electrojet, *(middle)* vertical plasma drift and *(bottom)* crest-to-trough ratio of the equatorial ionization anomaly.

Figure 3a: Filtered data of tidal signatures from the months around August: *(left)* zonal wavenumber 1, *(right)* wavenumber 2. Presented signals are: *(top)* the equatorial electrojet, *(middle)* vertical plasma drift and *(bottom)* the crest-to-trough ratio of the equatorial ionization anomaly.

Figure 3b: Same as Figure 3a, but for wavenumbers 3 and 4.

Figure 4: Annual variation of the diurnal nonmigrating tides DE2 and DE3: *(top)* the equatorial electrojet, *(middle)* vertical plasma drift and *(bottom)* the crest-to-trough ratio. The right column shows the amplitudes and the left the phases.

Figure 5: Annual variation of the relative modulation of the DE2 and DE3 tidal components: *(top)* equatorial electrojet intensity, *(middle)* vertical plasma drift and *(bottom)* crest-to-trough ratio.

Figure 6: Spectra of nonmigrating tidal signatures: *(top)* equatorial electrojet [mA/m], *(middle)* vertical plasma drift [m/s] and *(bottom)* crest-to-trough ratio. In the left column diurnal tides are shown and in the right semi-diurnal.

Figure 7: Comparison of the annual variation of the DE2 and DE3 tidal signatures in zonal wind at 100 km (top) and at ~400 km altitude (bottom). (TIMED zonal wind data courtesy of N. Pedatella)

Figure 8: Filtered signal of zonal wavenumber 4 in the vertical plasma drift for all local times. The thick dashed line marks the expected DE3 tidal phase propagation front. After midnight the amplitudes and phases vary randomly

Figures

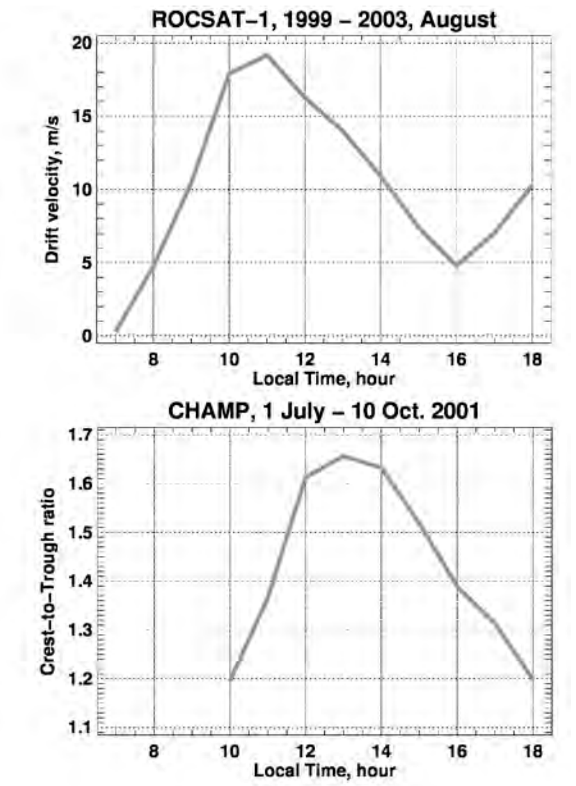

Figure 1: Zonally averaged diurnal variation: *(top)* vertical plasma drift, *(bottom)* crest-to-trough ratio of the equatorial ionization anomaly.

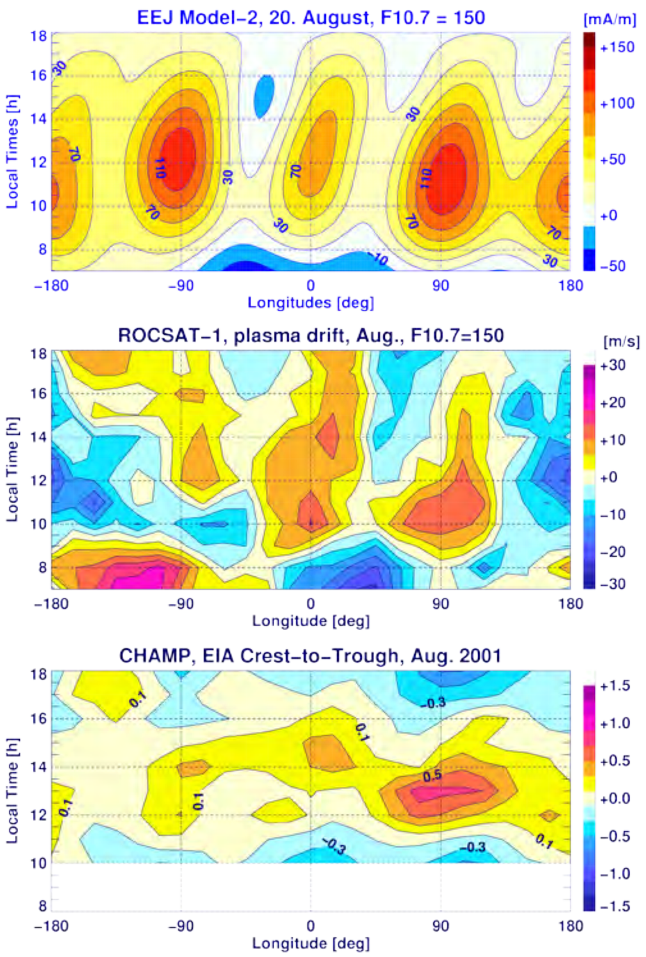

Figure 2: Local time dependence of the longitudinal variation during the months around August: *(top)* equatorial electrojet, *(middle)* vertical plasma drift and *(bottom)* crest-to-trough ratio of the equatorial ionization anomaly.

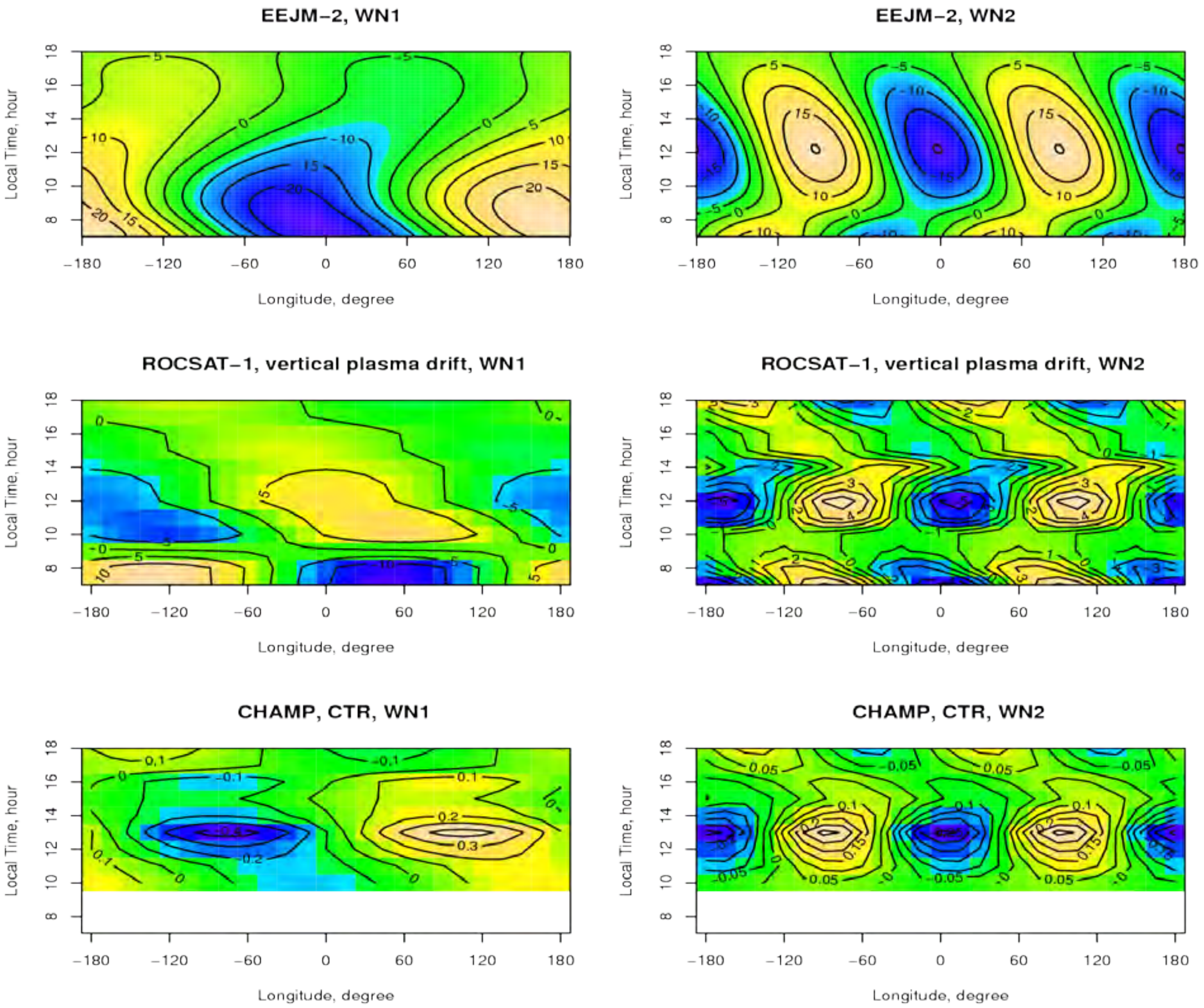

Figure 3a: Filtered data of tidal signatures from the months around August: *(left)* zonal wavenumber 1, *(right)* wavenumber 2. Presented signals are: *(top)* the equatorial electrojet, *(middle)* vertical plasma drift and *(bottom)* the crest-to-trough ratio of the equatorial ionization anomaly.

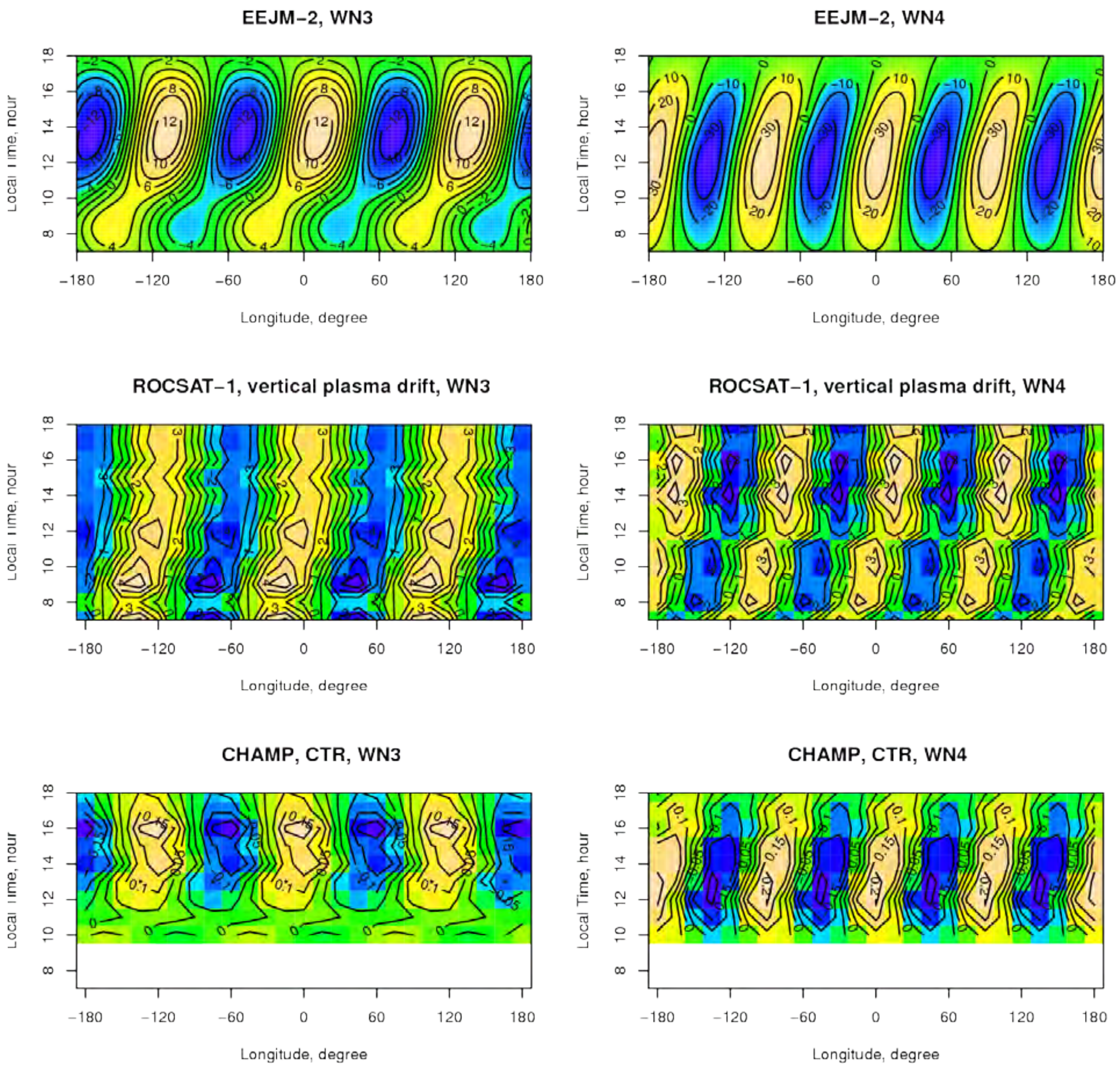

Figure 3b: Same as Figure 3a, but for wavenumbers 3 and 4.

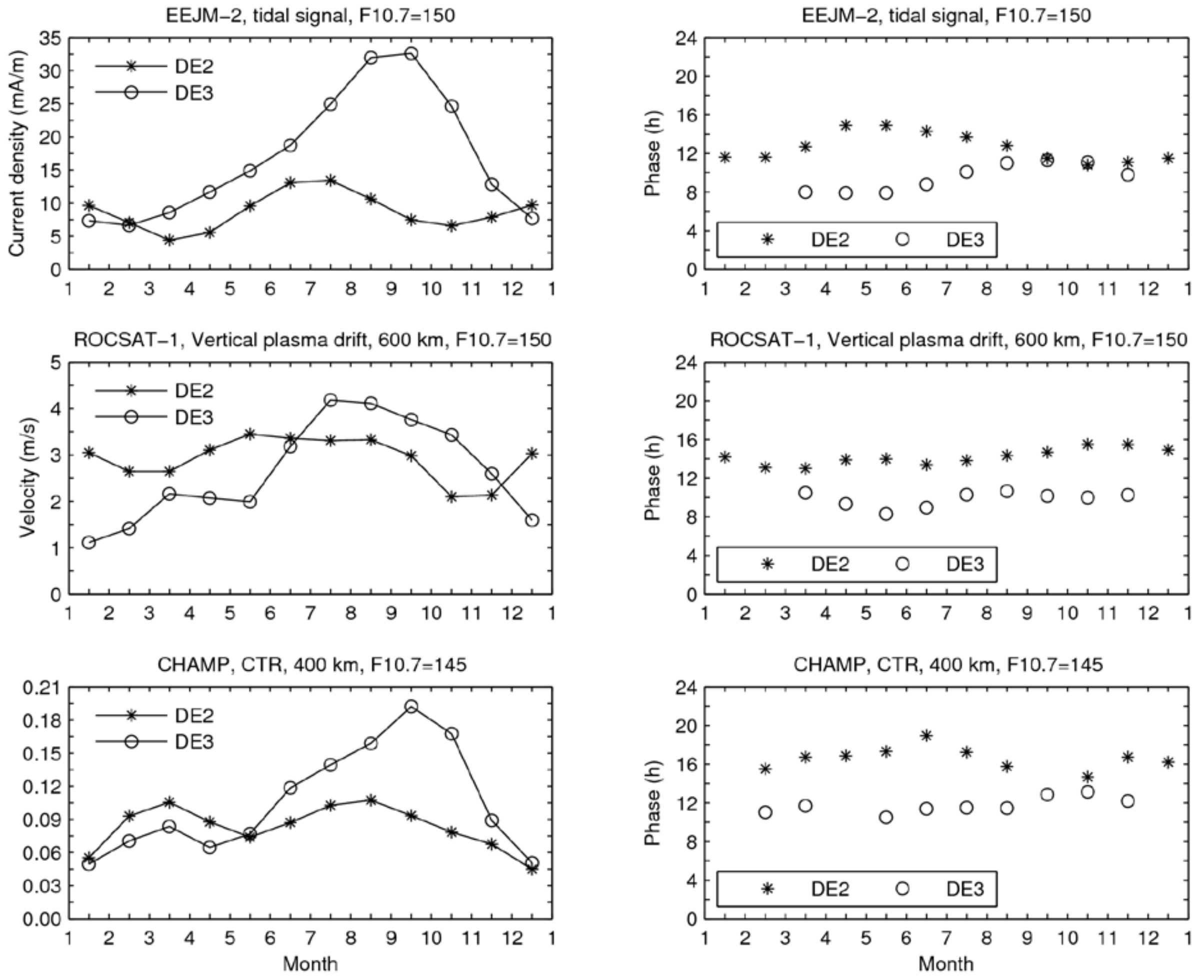

Figure 4: Annual variation of the diurnal nonmigrating tides DE2 and DE3: *(top)* the equatorial electrojet, *(middle)* vertical plasma drift and *(bottom)* the crest-to-trough ratio. The right column shows the amplitudes and the left the phases.

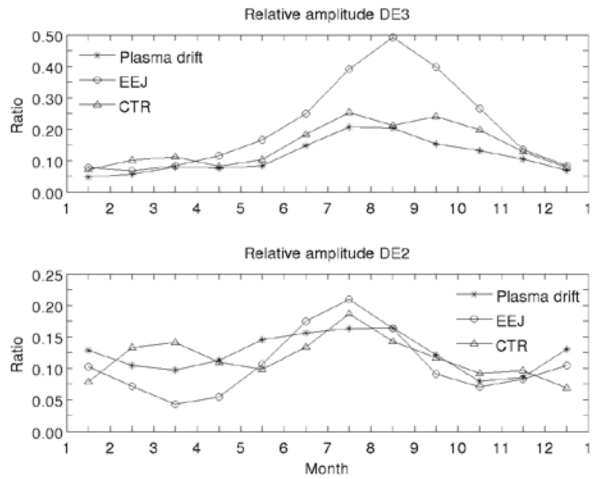

Figure 5: Annual variation of the relative modulation of the DE2 and DE3 tidal components: *(top)* equatorial electrojet intensity, *(middle)* the vertical plasma drift and *(bottom)* crest-to-trough ratio.

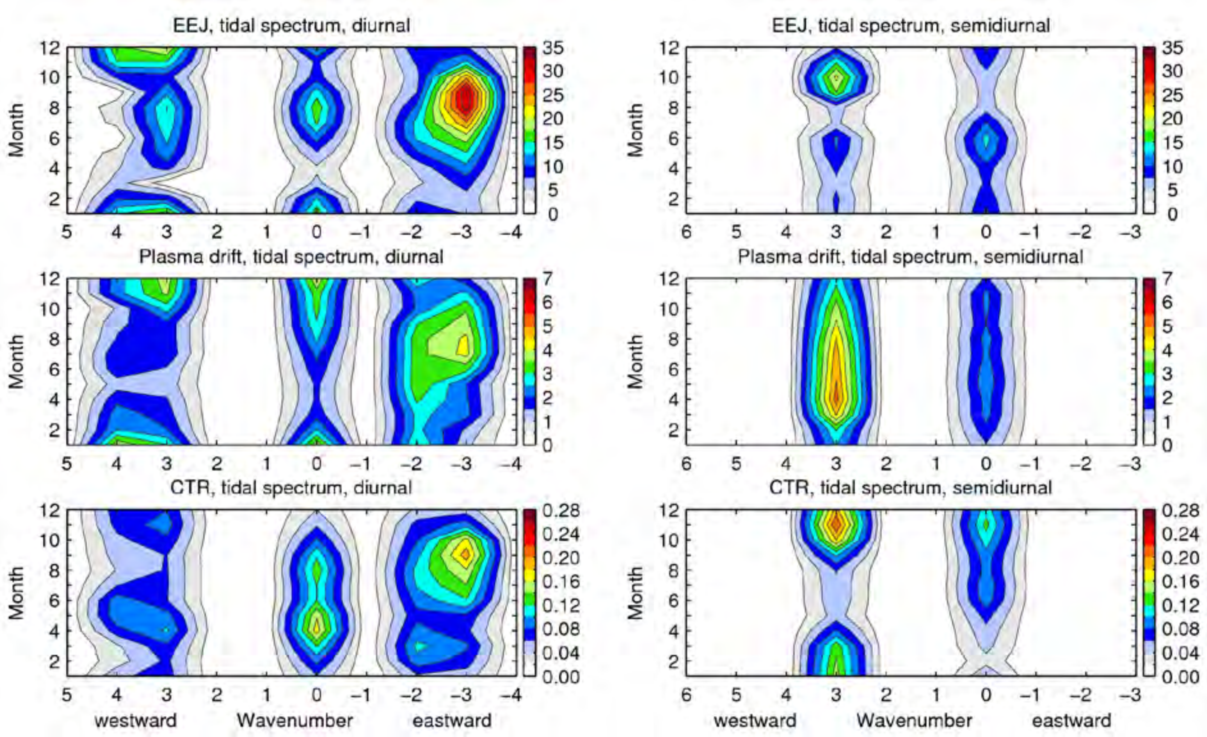

Figure 6: Spectra of nonmigrating tidal signatures: *(top)* equatorial electrojet [mA/m], *(middle)* vertical plasma drift [m/s] and *(bottom)* crest-to-trough ratio. In the left column diurnal tides are shown and in the right semi-diurnal.

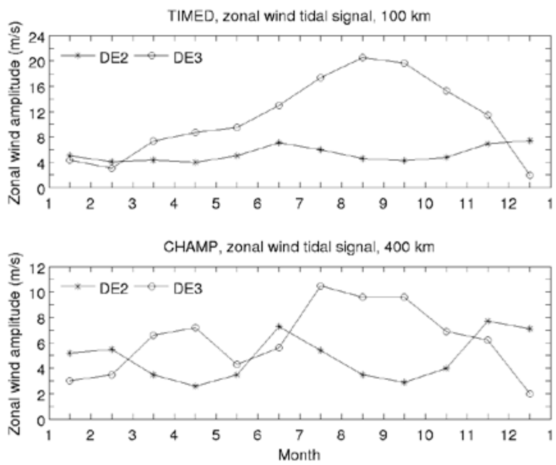

Figure 7: Comparison of the annual variation of the DE2 and DE3 tidal signatures in zonal wind at 100 km (top) and at ~400 km altitude (bottom). (TIMED zonal wind data by courtesy of N. Pedatella)

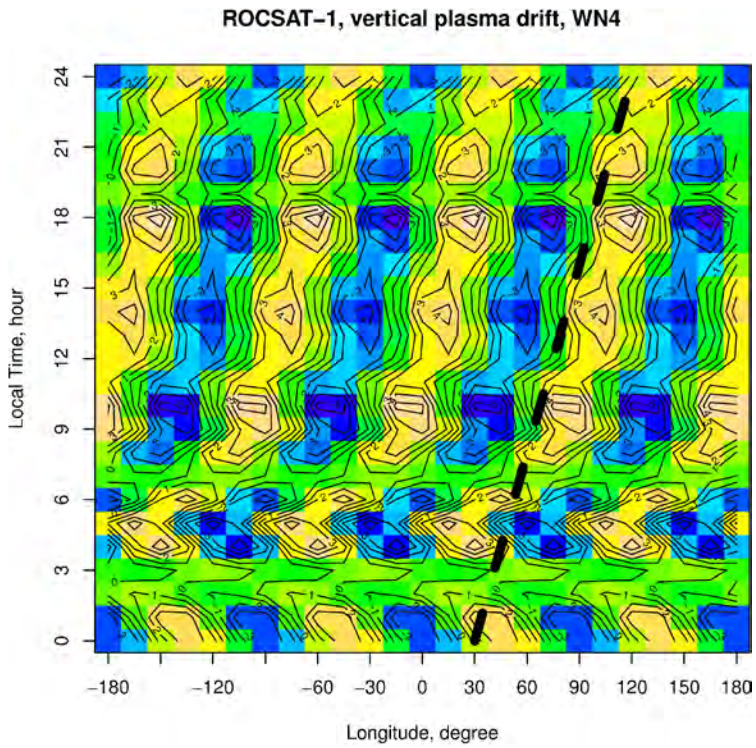

Figure 8: Filtered signal of zonal wavenumber 4 in the vertical plasma drift for all local times. The thick dashed line marks the expected DE3 tidal phase propagation front. After midnight the amplitudes and phases vary randomly.